Polym. Bull. (2017) 74:1611–1627
DOI 10.1007/s00289-016-1792-2

ORIGINAL PAPER

Enhanced thermal and mechanical properties of liquid crystalline-grafted graphene oxide-filled epoxy composites

Laifu Song[1] · Shaorong Lu[1] · Xiane Xiao[1] · Bo Qi[1] · Zihai He[1] · Xu Xu[1] · Baolin Rao[1] · Jinhong Yu[1,2]

Received: 23 December 2015 / Revised: 13 August 2016 / Accepted: 16 August 2016 /
Published online: 25 August 2016

Abstract Epoxy composites with biphenyl liquid crystalline polyester (BLCP)-grafted graphene oxides (GO) as inclusions were prepared successfully. The thermal and texture analyses of BLCP were characterized by DSC and POM. The results show that the texture structure of BLCP turned into fan texture from woven texture with increasing temperature and present double texture structure. More importantly, the thermal and mechanical properties of epoxy composites could be improved by incorporating BLCP-grafted GO (BLCP-GO). The epoxy composite with only 0.5 wt% BLCP-GO produced an increase in the initial decomposition temperature (T_d) by 28 °C and glass transition temperature (T_g) by 17.2 °C when compared with the neat epoxy. Moreover, for the mechanical properties tests, the composites with 1.0 wt% BLCP-GO exhibit an increase in impact strength, tensile strength, flexural strength and flexural modulus by 103, 52, 66, and 56 %, respectively, compared with the neat epoxy resin. These excellent performances of the graphene–epoxy composites have a great potential for applications in aerospace and other electrical devices.

Keywords Liquid crystalline · Graphene oxide · Epoxy composites · Thermal properties · Mechanical properties

✉ Shaorong Lu
lushaor@163.com

✉ Jinhong Yu
yujinhong@nimte.ac.cn

[1] Key Laboratory of New Processing Technology for Nonferrous Metals and Materials, Ministry of Education, School of Material Science and Engineering, Guilin University of Technology, Guilin 541004, China

[2] Key Laboratory of Marine Materials and Related Technologies, Zhejiang Key Laboratory of Marine, Materials and Protective Technologies, Ningbo Institute of Materials Technology and Engineering, Chinese Academy of Sciences, Ningbo 315201, China

Introduction

Currently, the study of nanofiller-reinforced polymeric materials has attracted more attention. A wide variety of fillers such as carbon nanotubes (CNTs), graphene and graphene oxide (GO), fullerenes, layered silicates and inorganic nanoparticles were added to polymer matrix which contributed to the enhancement of mechanical, thermal stability and gas barrier properties [1–4]. In contrast to the traditional inorganic nanoparticles (such as boron nitride, aluminum and silica, etc.) [5, 6], the functionalized graphene with layered structure can effectively reinforce the properties of the composite materials [7].

The GO was provided with remarkable mechanical and thermal properties attributed to their extremely high specific surface area which make them ideal candidates for the reinforcing phase in polymer nanocomposites [8, 9]. The GO is a chemically modified graphene which is decorated with hydrophilic oxygen functional groups, such as hydroxyl, epoxy, and carboxylic groups. Those hydrophilic functional groups make the GO to spontaneous stable dispersion in aqueous solution and organic solution of polarity [10–12]. Also, the surface modification of GO has turned into an important method which has not only improved the dispersion, but also improved a strong interface between GO and the matrix. And also many different functional groups can be introduced onto the graphene sheets [13]. Incorporation of these modified GO into polymer matrices can easily prepare a variety of excellent functional composites. Ge et al. [14] reported that triethylenetetramine-modified graphene oxide/chitosan composite was synthesized by microwave irradiation method which could significantly improve adsorption of Cr in effluents, and highest adsorption capacity of Cr reaches up to 219.5 mg g^{-1}. Ribeiro et al. [2] indicated that the chemical modification of the GO by TEPA had improved the thermal and mechanical properties of composites. The type and extent of chemical modification of GO are the critical factors. Fan et al. [15] showed that GO is converted into graphene by the chemical modification using alkyl imidazolium ionic liquids (ILs) as lubricant additives to greatly enhance friction and anti-wear behaviors.

Liquid crystals polymer (LCP) as the functional of soft materials has attracted considerable attention in recent decades. With regard to future developments, the main attention is not only focused on academia but also on industry application due to its excellent thermal stability, excellent mechanical and photoactive [16–20]. In particular, thermotropic main-chain LCP copolyester is significantly important to the polymer's transverse strength and compressive strength. It represents a class of high-tech polymers which combine high mechanical performances with low density [21, 22]. Noteworthily, polymer composites with LCP improved toughness, thermal conductivity, and other thermal properties without sacrificing other performance. These outstanding properties provide the opportunity to be used widely in applications such as aerospace, energy storage and electronic packaging [23–26].

Epoxy resin as one of the most important typical polymer matrices in composite has drawn attention due to its excellent mechanical properties, good thermal stability and low shrinkage [27, 28]. Hence, it is used widely in industry

applications including structural materials, adhesives, coatings and additive-type flame retardant [29]. However, cross-linked resins generally have weak resistance to crack propagation and low fatigue resistance to heat and impact due to the inherent brittleness, which limited the effective usage of epoxy composites [30, 31]. The functionalized GO can effectively improve the properties of epoxy resins, such as toughness, glass transition temperature and impact resistance without sacrificing their intrinsic properties [32–34].

The aim of this study is to develop a new functionalized GO which was modified by biphenyl liquid crystalline polyester (BLCP-GO) as a reinforcing filler to improve the mechanical and thermal properties of epoxy. The BLCP-GO dispersed in the epoxy resins to form the crosslinking networks in the curing reaction. Meanwhile, BLCP-GO are chosen as the fillers for preparing the epoxy composites with 0.5, 1.0, 1.5, and 2.0 wt% BLCP-GO loading. The epoxy composites have been characterized in terms of their morphological, thermal, and mechanical properties to study the effect of the BLCP-GO on their dispersion in the epoxy matrix and the interaction with the epoxy.

Experimental

Materials

The epoxy resin used in this study is diglycidylether of bisphenol A (DGEBA, E-51, epoxy value = 0.51 and viscosity value = 12 Pa s at 25 °C) supplied by Yueyang Chemical Plant (Yueyang, China). Nature graphite flake (325 mesh, 99 %) was purchased from Hengrui Graphite Co., Ltd. (Qingdao, China). H_2SO_4 (98 %), HCl (36 %), H_2O_2 (30 %), $KMnO_4$, KI, NaOH, P_2O_5 and $K_2S_2O_8$ were provided by Sinopharm Chemical Reagent Co., Ltd. (Shanghai, China). *N*, *N*′-Dimethylformamide (DMF), 4,4′-dihydroxydiphenyl sulfone (DDS) and pyridine were obtained from Xiya Chemical Reagent Co., Ltd. (Chengdu, China). 4-Dimethylaminopyridine (DMAP), *p*-phthaloyl chloride, 6-chloro-1-hexanol, and *N*,*N*′-diisopropylcarbodiimide (DIC) were purchased from Aladdin Chemistry Co., Ltd. (Shanghai, China). Deionized (DI) water was used in all the process of aqueous solution preparations and washings. All of the reagents were at analytical grade without further purification.

Synthesis of the biphenyl liquid crystalline polyester (BLCP)

The synthetic route of the 4,4′-di(6-hydroxy hexyloxy) biphenyl (BP_6) is described as Scheme 1. The BP_6 was synthesized by the nucleophilic substitution reaction of 4,4′-dihydroxydiphenyl and 6-chloro-1-hexanol in a molar ratio of 1:4. Briefly, NaOH (1.60 g, 0.04 mol), KI (1.66 g, 0.01 mol) as catalyst and 90 ml anhydrous ethanol solvent were added into a 250-ml three-necked, round-bottomed flask equipped with magnetic stirrer and thermometer [35]. After NaOH was completely dissolved under electromagnetic stirring, 4,4′-dihydroxydiphenyl (3.72 g, 0.02 mol) was added into the flask. Then, 6-chloro-1-hexanol was slowly dropped into the

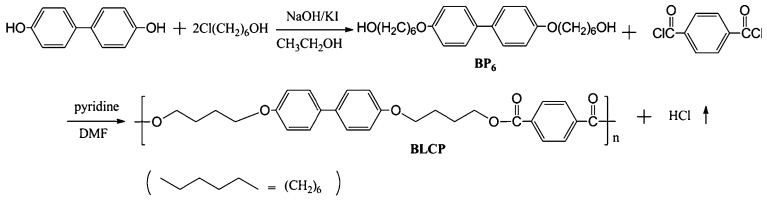

Scheme 1 The synthetic routes of the BLCP

above-mentioned mixture and heated to 75 °C for 24 h. After the reaction, the solution was cooled to room temperature. The precipitate was collected by filtration and then washed with distilled water (DI) several times. The crude product was recrystallized with DMF and was separated by filtration and vacuum-dried at 60 °C to obtain a white, needle-like crystal (BP_6).

In a three-necked flask, 4.25 g (0.011 mol) BP_6 was dissolved with 90 ml DMF solvent and 1 ml pyridine as catalyst was dropped into the mixture under stirring. p-phthaloyl chloride (2.03 g, 0.01 mol) was dissolved in 10 ml DMF and slowly dropped into the reaction solution to keep stirring at ambient temperature for 2 h, and then further reacted at 80 °C for another 12 h. The cold reaction mixture was precipitated into distilled water. The solid was washed with distilled water and then dried at 60 °C in a vacuum drying oven to provide the yellow powder.

Synthesis of BLCP-grafted graphene oxide (BLCP-GO)

The GO were prepared according to the modified Hummers method, in which the natural graphite flakes were oxidized in concentrated sulfuric acid, phosphorus pentoxide, potassium permanganate and hydrogen peroxide [19, 36, 37]. The GO suspensions were prepared via ultrasonication to form colloidal aqueous solutions and freeze-dried as shown in Scheme 2. Then, 0.1 g GO was dispersed in 100 ml DMF under ultrasonication for 30 min and was placed in a 250-ml three-necked flask. After that, 5 g BLCP, 2 g DIC and 0.05 g DMAP were placed in the above-mentioned mixture at ambient temperature and kept stirring for 2 h, and then heated to 40 °C for 48 h. After filtration, the crude product of the BLCP grafted-GO (BLCP-GO) was washed several times with DMF to ensure the complete removal of the free BLCP, then with ethyl alcohol to remove residues of DMF solvent, and the filtered material was dried in a vacuum oven at 60 °C.

Preparation of BLCP-GO/epoxy composites

The BLCP-GO/epoxy composites were prepared as follows: a specific amount of BLCP-GO as filler was dispersed in acetone and treated with ultrasound for 1 h. Then, the BLCP-GO dispersion was added to a stoichiometric amount of preheated epoxy. The mixture was heated up to 60 °C with stirring under the condition of vacuum to ensure the removal of the acetone solvent entirely and uniform dispersion. After that, curing agent DDS (30 g/100 g of epoxy resin) was added under vigorous mechanical stirring. Then, the mixture was poured into mold and

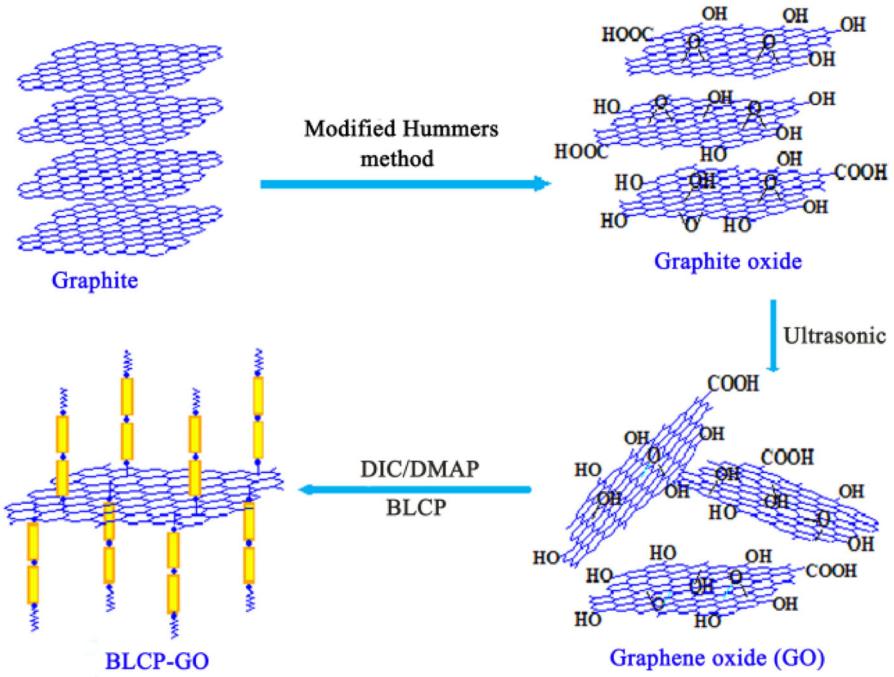

Scheme 2 The synthetic routes of biphenyl liquid crystalline polyester grafted GO

placed in a vacuum oven to remove air bubbles for 30 min. Finally, the mold was placed in a convection oven to cure at 140 °C for 2 h, 160 °C for 2 h and 180 °C for 2 h. The epoxy composites were prepared with different weight fractions (0, 0.5, 1.0, 1.5, and 2.0 wt%) of BLCP-GO by above methods.

Characterization

Fourier-transformed infrared spectroscopy (FTIR) was recorded between 4000 and 450 cm^{-1} on a Nicolet 470 spectrophotometer (spectra resolution: 0.125 cm^{-1}, 32 scans) using KBr pellets at room temperature. The morphology of composites was examined using field emission scanning electron microscopy (FE-SEM, JSM-6701F, Japan) at an accelerating voltage of 20 kV, and the cryogenic fractured surfaces of composites were sputter-coated with gold–palladium alloy before viewing. The liquid crystalline transitions and optical textures were observed using a Leica DMxRP polarizing microscope with an INSTEC STC-200 hot stage. Small amounts of samples (2–3 mg) were pre-melted on a microscope slide, then covered with a piece of cover glass to form a uniform thin film. The formation and development of the LC phase were examined under polarized light. Thermal gravimetric analysis (TGA) was performed with a NETZSCH STA 449C at a heating rate of 20 °C min^{-1} from 50 to 700 °C under nitrogen atmosphere. Differential scanning calorimetry (DSC-204, NETZSCH, Germany) was performed at temperature from 30 to 250 °C at a heating rate of 10 °C min^{-1}. All tests were

performed in a nitrogen atmosphere with a sample weight of about 8 mg. Dynamic mechanical analysis (DMA) was performed on DMA Q800 (TA Instruments, USA), operating in a single cantilever bending mode at an oscillation frequency of 1 Hz and displacement amplitude of 10 μm. Testing temperature was set as from room temperature to 250 °C at a heating rate of 3 °C min^{-1}. The impact strength was measured on a tester of type XJJ-5, which is with no notch in the specimen according to National Standard of China (GB1043-79). The specimen was with a thickness of 4 mm and width of 10 mm and length of 80 mm. The tensile strength was examined on an electron omnipotence tester of type RGT-5. The tensile experiments was used a three-point bending mode of the universal testing machine with a crosshead speed of 2 mm/min according to the National Standard of China (GB1040-92). All the presented results are an average of five specimens.

Results and discussion

Characterization of the fillers

FTIR spectra of the GO, BLCP and BLCP-GO are shown in Fig. 1. It can be seen in the three infrared curves, the wide and strong absorption peak at 3405 cm^{-1} attributed to hydroxyl group (–OH) stretching [8]. For the GO, the peak at 1722 and 1621 cm^{-1} was associated with the C=O carbonyl bending and the peak adsorption of water [38]. At 1384 $cm^{-1}$was presented a strong and sharp peak corresponding to hydroxyl vibration. A peak appearing at 1150 cm^{-1} is associated with the C–O stretching vibration of the epoxy group. For the spectrum of BCLP, the peaks at 2865 and 2938 cm^{-1} could be attributed to $–CH_2$ symmetrical and asymmetrical stretching vibrations. The band of 1690 cm^{-1} is due to the C=O stretching. The

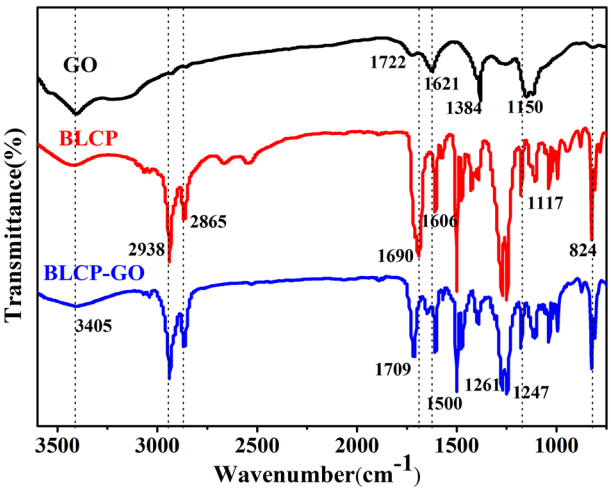

Fig. 1 FT-IR spectra of GO, BLCP and BLCP-GO

bands at 1606, 1500 and 824 cm^{-1} were due to aromatic structure [35, 39]. The bands at 1261 and 1247 cm^{-1} were associated with the $–CH_2$ out-of-plane bending vibration. Comparing the spectra of GO and BLCP with that of BLCP-GO, it was found that the characteristic absorption peaks of the BLCP appear on the spectrum of product BLCP-GO. The original peak of GO curve at 1722 cm^{-1} disappeared. However, a new peak was observed at 1709 cm^{-1}. This is due to carboxyl group of GO by modification into the ester group. The peak at 1621 cm^{-1} disappeared in the GO curve due to some oxygen-containing functional groups included in the reaction process and the liquid crystal molecules that inhibit water.

The thermal behaviors and liquid crystal properties of synthesized BP_6, BCLP were investigated by differential scanning calorimetry (DSC) and polarizing optical microscope (POM) in Fig. 2. The DSC heating curve of BP_6 shows two distinct endothermic sharp peaks at 99.1 and 176.5 °C. They correspond to the BP_6 melting temperature (T_m) and isotropization temperature (T_i), respectively. It revealed the change of a crystalline solid into the liquid crystalline state at 99.1 °C (T_m), and then the temperature reached to 176.5 °C (T_i), which is the liquid crystalline structure to isotropic phase. The image of POM showed that the sample of BP_6 began to melt and gradually turned to fan of liquid crystal texture when it was heated to 110 °C which is in inset of Fig. 2a. The texture disappears and the isotropic phase was observed above 185 °C. Furthermore, the phase transition temperatures observed by POM are conformed to the DSC determination results. It can be confirmed that the presence of obvious liquid crystalline mesophases for these BP_6 and it exhibited relatively wide temperature range of the liquid crystal phase. This is attributed to the long flexible chain on both sides of the biphenyl, which is easy to orientation [35, 40]. For the DSC curve of BLCP which is shown in Fig. 2b, three endothermic peaks appear in the field of vision, which correspond to melting point temperature (at 99.9 °C), texture transformation temperature (at 134.7 °C) and clearing point of temperature (at 151.4 °C). The POM observation of BLCP indicated that the sample shows bright fine-grain woven structures after melting (inset I). With increasing temperature, woven texture structures suddenly turn into fan texture structure (inset

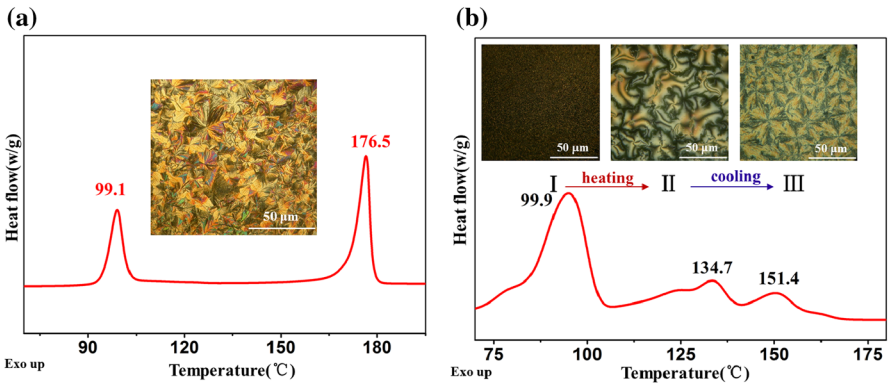

Fig. 2 **a** DSC curve of BP6, *inset* POM figure of BP6; **b** DSC curve of BLCP, *inset* POM figures of BLCP

II) and subsequently, the liquid crystalline phases of sample disappeared and turned into isotropic phase [41, 42]. The similar woven texture structures can be observed when it was cooled (inset III). Also, POM and DSC results are consistent.

The TGA curves of GO, BLCP, and BLCP-GO under nitrogen and air atmosphere are shown in Fig. 3. Under nitrogen atmosphere, as shown in Fig. 3a, it was also found that the GO weight loss about 12 wt% at 100 °C, which is due to evaporation of the remaining water. However, BLCP-GO has no loss of weight at this stage. It means that introduction of BLCP will reduce the ability of absorbed water. After that, GO was loss of weight sharply about 28 wt% between 160 and 220 °C, which was attributed to the decomposition of labile oxygen groups [12] to produce H_2O, CO, CO_2. Compared with the GO, the weightlessness of BLCP-GO has weakened. This is mainly due to the removal of the oxygen groups residual of the GO [38]. At higher temperatures, the decomposition temperatures (T_d) of BLCP and BLCP-GO are 275 and 365 °C, respectively. The T_d of the BLCP-GO is 90 °C higher than that of BLCP. The degradation mechanism of BLCP and BLCP-GO is the fracture of C–C bond and C–O bonds, to produce massive quantities of molecules such as oligomers, low-molecular polyester, low alkane, hexylidene, CO, CO_2 etc. These results suggest that the thermal stability of the GO has been improved after modification with BLCP. This is because the oxygenic groups of GO have been replaced by BLCP chain to form a stable chemical bond, and they strongly interacted with GO sheets leading to the decrease of the molecular motion and the increase of the rupture temperature of the polymer backbone. However, under air atmosphere, as shown in Fig. 3b, the thermal stability of BLCP-GO has deteriorated. The thermal decomposition temperature drops and residual carbon amount is only 6 wt%.

Figure 4 shows the SEM images of GO and BLCP-GO nanosheets. It can be seen from Fig. 4a that the GO are showing transparent and overlapping in some instances. Corrugation and scrolling are parts of the intrinsic nature of GO, which result from the fact of the two-dimensional membrane structure becoming thermodynamically stable via bending. The SEM image of BLCP-GO are shown

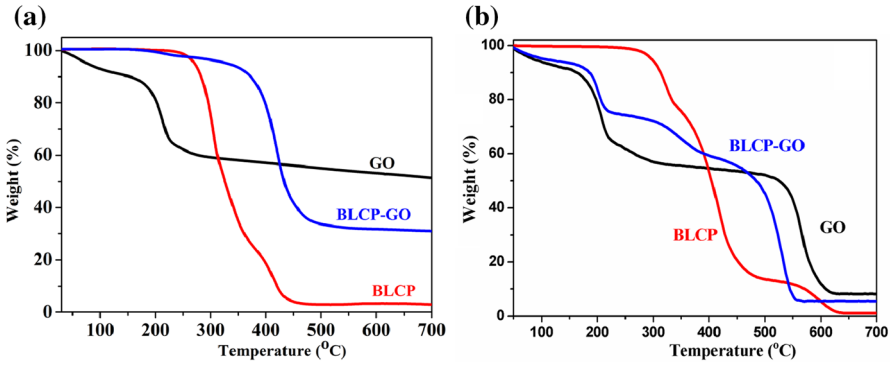

Fig. 3 TGA curves of GO, BLCP and BLCP-GO under **a** N_2 and **b** air atmosphere

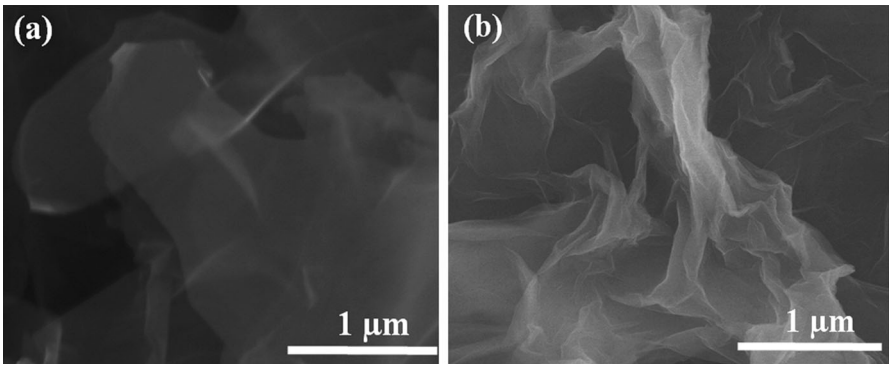

Fig. 4 SEM image of **a** GO and **b** BLCP-GO

in Fig. 4b. It can be found that some obvious BLCP were grafted to the GO nanosheets leading to loss of transparency.

Morphology of composites

Figure 5 shows the SEM images of the impact fracture surfaces of neat epoxy and the BLCP-GO/epoxy composites. It can be seen that Fig. 5 provides three groups of representative images with different magnification. The fracture surface of the neat epoxy exhibits river patterns observed from Fig. 5a, b. Also, fracture surface was very smooth and single crack direction, which indicates that neat epoxy almost presents no plastic deformation and weak resistance to crack initiation. This is a typical brittle fracture and consistent with poor tensile strength [6, 22, 43]. The fracture surfaces of 1.0 wt% BLCP-GO/epoxy composites are shown in Fig. 5c, d. The fracture surface is very rough, which presents uneven or fuzzy interface and spreads the crack extension. The reason is that BLCP-GO hinders crack extension to make materials ductile fracture. This indicates that the addition of modified GO changes the way fracture of epoxy resin. GO flake linked the substrate together like a bridge, leading to the flexible interface and discouraging the formation of brittle fracture [31, 44, 45]. At the same time, the rigid segment structure of liquid crystal acting as a steel reinforcement exhibited ductile behavior when the material ruptured. However, with the filler loading increasing, BLCP-GO nanosheets exist in the form of agglomerates and affect uniformity of material as shown in Fig. 5e, f.

Thermal properties of epoxy composites

Figure 6 shows the TGA and DTG curves of neat epoxy and its composites. As can be seen from the curves, all of the samples present a single thermal decomposition platform and exhibit similar thermal behavior, which means that the addition of BLCP-GO does not change the degradation mechanism of epoxy matrix. It can be seen that initial decomposition temperature of neat epoxy at 351 °C in Fig. 6a. Compared with neat epoxy, the decomposition temperature (T_d) of the composite

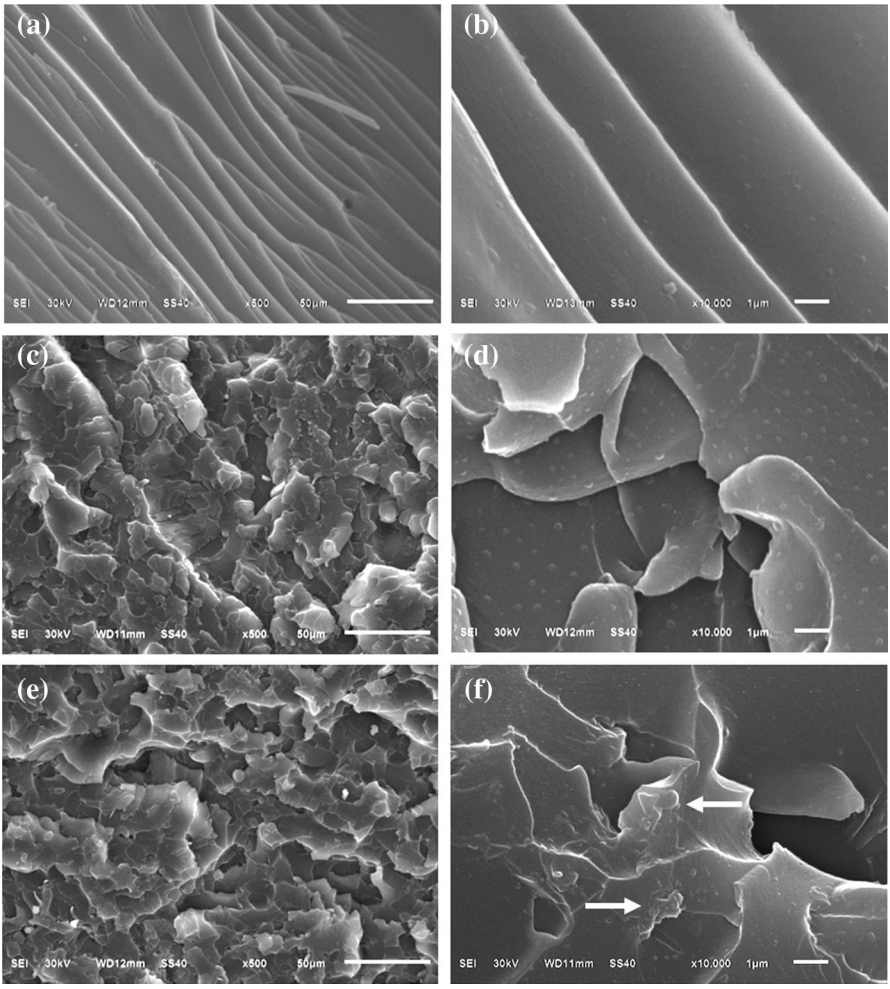

Fig. 5 SEM images of fractured surface of composites: **a**, **b** neat epoxy, **c**, **d** 1.0 wt%; and **e**, **f** 2.0 wt%

materials has improved when the modified GO was added into the epoxy matrix. The T_d of composites increases by 28 °C when BLCP-GO content is 0.5 wt%. As DTG curves shown in Fig. 6b, the composite with 0.5 wt% content of BLCP-GO has the maximum degradation temperature at 421 °C [46, 47]. The decomposition temperatures (T_d) and the maximal decomposition temperature (T_{max}) are listed in Table 1. Thermal properties data indicated that the addition of BLCP-GO improves the thermal property of epoxy composites. It can be attributed to two factors. First, the BLCP-GO sheets act as physical interlock points and physical tangles with the epoxy matrix, thus hindereing the thermal motion of epoxy matrix molecule [28]. Second, the crosslinking between nanosheets and epoxy groups in the curing reaction restrained the mobility of chain, which leads to enhanced thermal properties of the composites [48, 49].

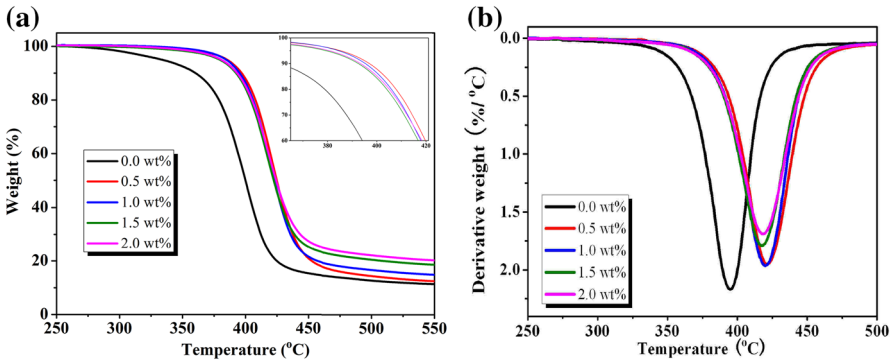

Fig. 6 **a** TGA and **b** DTG curves of the neat epoxy and its composites, *inset* in **a**: drawing of partial enlargement

Table 1 Thermal stabilities of epoxy composites

The content of BLCP-GO (wt%)	Decomposition temperature (T_d)	Maximum decomposition temperature (T_{max})
0.0	355	396
0.5	383	421
1.0	382	420
1.5	377	418
2.0	377	418

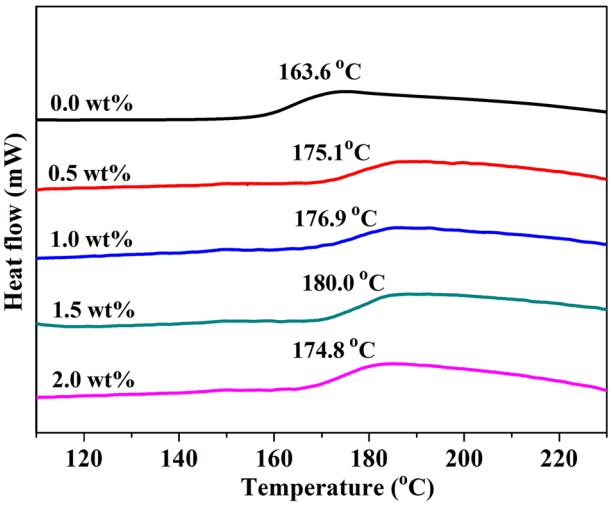

Fig. 7 DSC curves of the neat epoxy and epoxy composites

Figure 7 shows the DSC curves for neat epoxy and its composites, which exhibit the change in T_g for composites. It can be seen that the T_g of pristine epoxy takes place at 163.6 °C. The addition of BLCP-GO nanosheets can enhance the T_g of the epoxy composites, which shifts to a higher temperature compared to neat epoxy. The T_g values of the BLCP-GO/epoxy composites with 0.5, 1, 1.5, and 2 wt% BLCP-GO fillers are 175.1, 176.9,180 and 174.8 °C, respectively. The maximum value of T_g is 16.4 °C higher than that of the neat epoxy resin when the filler content is 1.5 wt%. It's attributed to good interaction between the nanosheets and epoxy matrix. When the filler content is higher than 1.5 wt%, the T_g of the BLCP-GO composites was decreased with increasing the content of BLCP-GO filler. The main reason was BLCP-GO agglomerate in the epoxy matrix. Once nanosheets agglomerate, the interactions are more between BLCP-GO nanosheets rather than BLCP-GO nanosheets and epoxy matrix. The agglomerated BLCP-GO nanosheets could not impose any restrictions on the mobility of epoxy, and thereby higher loading BLCP-GO nanosheets resulting in lower T_g values. But the T_g values of BLCP-GO composites with 2.0 wt% are still higher than that of neat epoxy at higher filler content.

The storage modulus and tan δ of neat epoxy and its composites were measured by DMA to study the effects of BLCP-GO filler in Fig. 8. The incorporation of the BLCP-GO filler did not deteriorate the thermomechanical behavior. Within the experimental temperature range, the storage modulus of epoxy composites is higher than that of neat epoxy. It reflected the interface interaction between BLCP-GO filler and epoxy resin matrix flexibility and effectively. As shown in Fig. 8a, the storage modulus of the epoxy was increased by the addition of the BLCP-GO fillers, especially in the glass region. In the test temperature range, all the storage modulus of the composites was much higher than that of neat epoxy but exhibited irregular change with increasing of the loading fillers. It is attributed to the inherent hardness and strong storage modulus of filler. Well-dispersed BLCP-GO fillers filled the spaces in the epoxy matrix and acted as the crosslinking points. On one hand, the high surface area of hybrid fillers has a huge interface with epoxy resin matrix and provides an effective way to transfer the actual stress from the matrix. On the other hand, the LC domains of filler participate in crosslinking networks with the matrix

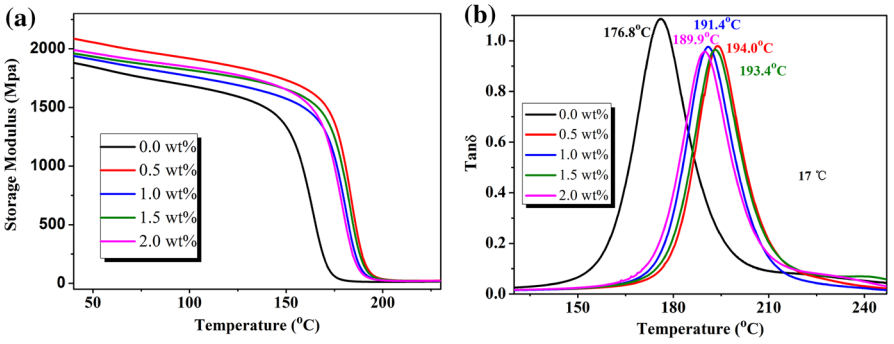

Fig. 8 **a** Storage modulus and **b** tan δ of the neat epoxy and epoxy composites

to form strong covalent bonding leading to hinder the movements of the polymer chains [2, 47, 48]. Figure 8b shows the tan δ curve of neat epoxy and its composites. The T_g of neat epoxy and its' composites could be obtained accurately from the tan δ peaks. The T_g of the BLCP-GO/epoxy composites with 0, 0.5, 1.0, 1.5, and 2.0 wt% are 176.8, 194.0, 191.4, 193.4 and 189.9 °C, respectively. The variation trend of T_g measured by DMA shows a slight distinction with the results of DSC. The main reason for the discrepancy is based on two different principles measurement of T_g. There are different T_g results between DSC and DMA. For DMA measurement, the highest T_g value is up to 194.0 °C at 0.5 wt%, which increased by 17.2 °C compared to the neat epoxy. The filler effect and the crosslink effect can improve the thermal stability of the composite materials [50]. On the other hand, the free volume of the composites was significantly reduced when the BLCP-GO filler was added.

Mechanical properties of epoxy composites

Figure 9 shows the impact strength and tensile strength of neat epoxy and its composites with different content. As can be seen from it, the impact strength and tensile strength of composite materials were obviously improved with the addition of BLCP-GO. Within a certain content of BLCP-GO, the impact strength and tensile strength were improved steeply with the increasing of BLCP-GO and reached the maximum, then decreased again at higher loading. The peaks of impact strength and tensile strength reached the maximum with content of 1.0 and 1.5 wt% BLCP-GO, which improved by 103 and 60 % compared to neat epoxy, respectively [43]. Two reasons may account for this phenomenon. First, this is attributed to provide an effective way that the actual stress is expected to be easily transferred from the matrix to GO nanosheets. Second, the residual epoxy groups of GO form the chemical crosslinking with epoxy matrix, which hinders the stress concentration effect to improve impact strength and tensile strength [51, 52].

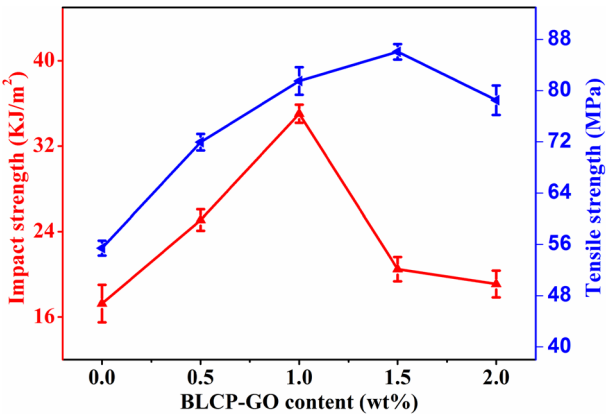

Fig. 9 Impact strength and tensile strength of neat epoxy and epoxy composites

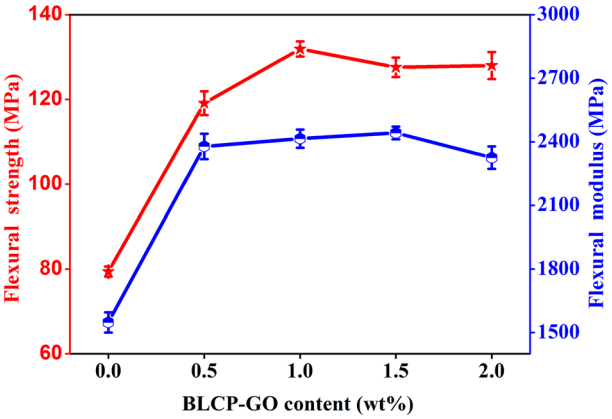

Fig. 10 Flexural strength and modulus of neat epoxy and its composites

Table 2 The mechanical properties of neat epoxy and its composites

The content of BLCP-GO (wt%)	Impact strength (KJ/m^2)	Tensile strength (MPa)	Flexural strength (MPa)	Flexural modulus (MPa)
0.0	17.26	53.65	79.4	1548
0.5	25.08	71.95	119.1	2378
1.0	35.03	81.50	131.9	2415
1.5	20.49	86.06	127.6	2442
2.0	19.09	78.50	128.0	2325

Figure 10 shows the flexural strength and modulus of the neat epoxy and its composites. The results show an improvement in strength and modulus of the composites compared to neat epoxy with increasing of BLCP-GO but the change trend is different. For instance, the maximum flexural strength (131.9 MPa) and modulus (2442 Mpa) were observed in 1.0 and 1.5 wt% BLCP-GO content, respectively, which increased by 66.1 and 57.8 % compared to neat epoxy [19, 51]. However, the flexural properties of the epoxy composites decreased when the filler loading exceeds the critical level. The mechanical properties of the epoxy composites were enhanced due to the good compatibility between BLCP-GO and epoxy matrix, which has good dispersion and is beneficial for the efficient stress transfer in epoxy matrix [13]. Table 2 summarizes the mechanical properties data.

Conclusions

Epoxy composites with BLCP-GO as inclusions were prepared successfully. The epoxy composites have excellent thermal and mechanical properties due to the strong interfacial interaction. The epoxy composite with only 0.5 wt% BLCP-GO

increased the initial decomposition temperature (T_d) by 28 °C and glass transition temperature (T_g) by 17.2 °C comparing with neat epoxy. Meanwhile, the composites with the 1.0 wt% BLCP-GO exhibit an increase in impact strength, tensile strength, flexural strength and flexural modulus by 103, 52, 66 and 56 %, respectively. This work clearly indicates that the novel BLCP-GO fillers play a critical role in the improvement of epoxy composites.

Acknowledgments The authors gratefully acknowledge the financial support by National Natural Science Foundation of China (51303034, 51367007, 51463007, and 51573201), the Natural Science Foundation of Guangxi Province, China (2014GXNSFDA118006, 2014GXNSFBA118034 and 2015GXNSFBA139231), Guangxi Universities Scientific Research Project (No. YB2014165), Natural Science Foundation of Ningbo (No. Y40307DB05) and International Science and Technology Cooperation Program of Ningbo (No. 2015D10003), Guangxi Ministry-Province Jointly-Constructed Cultivation Base for State Key Laboratory of Processing for Non-ferrous Metal and Featured Materials (15AA, 13KF-4).

References

1. Huang ZD, Liang R, Zhang B et al (2013) Evolution of flexible 3D graphene oxide/carbon nanotube/polyaniline composite papers and their supercapacitive performance. Compos Sci Technol 88:126–133
2. Ribeiro H, da Silva WM, Neves JC et al (2015) Multifunctional nanocomposites based on tetraethylenepentamine-modified graphene oxide/epoxy. Polym Test 43:182–192
3. Lim MY, Oh J, Kim HJ et al (2015) Effect of antioxidant grafted graphene oxides on the mechanical and thermal properties of polyketone composites. Eur Polym J 69:156–167
4. Jeong YG, An JE (2014) Microstructure and electrical property of epoxy/graphene/MWCNT hybrid composite films manufactured by UV-curing. Macromol Res 22(10):1059–1065
5. Chung SC, Hahm WG, Im SS et al (2002) Poly(ethylene terephthalate)(PET) nanocomposites filled with fumed silicas by melt compounding. Macromol Res 10(4):221–229
6. Yu JH, Huo RM, Wu C et al (2012) Influence of interface structure on dielectric properties of epoxy/alumina nanocomposites. Macromol Res 20(8):816–826
7. Vennerberg D, Hall R, Kessler MR (2014) Supercritical carbon dioxide-assisted silanization of multi-walled carbon nanotubes and their effect on the thermo-mechanical properties of epoxy nanocomposites. Polymer 55(16):4156–4163
8. Xu M, Huang Q, Wang X et al (2015) Highly tough cellulose/graphene composite hydrogels prepared from ionic liquids. Ind Crops Prod 70:56–63
9. Basnet S, Otsuka M, Sasaki C et al (2015) Functionalization of the active ingredients of Japanese green tea (Camellia sinensis) for the synthesis of bio-based epoxy resin. Ind Crops Prod 73:63–72
10. Gadipelli S, Guo ZX (2015) Graphene-based materials: synthesis and gas sorption, storage and separation. Prog Mater Sci 69:1–60
11. Senthilnathan J, Liu YF, Rao KS et al (2014) Submerged liquid plasma for the synchronized reduction and functionalization of graphene oxide. Sci Rep 4:4395
12. Fang M, Wang KG, Lu HB et al (2009) Covalent polymer functionalization of graphene nanosheets and mechanical properties of composites. J Mater Chem 19(38):7098–7105
13. Ramezanzadeh B, Ghasemi E, Mahdavian M et al (2015) Characterization of covalently-grafted polyisocyanate chains onto graphene oxide for polyurethane composites with improved mechanical properties. Chem Eng J 281:869–883
14. Ge H, Ma Z (2015) Microwave preparation of triethylenetetramine modified graphene oxide/chitosan composite for adsorption of Cr(VI). Carbohydr Polym 131:280–287
15. Fan X, Wang L (2015) High-performance lubricant additives based on modified graphene oxide by ionic liquids. J Colloid Interface Sci 452:98–108
16. Mija A, Navard P, Peiti C et al (2010) Shear induced structuration of liquid crystalline epoxy thermosets. Eur Polym J 46(6):1380–1387

17. He X-Z, F-d Zhang, Jia Y et al (2015) Branched-arm macromolecule liquid crystals-containing fluorine and isosorbide-structure and properties. J Mol Struct 1092:96–103
18. Didehban K, Namazi H, Entezami AA (2010) Non-covalent dendrimer-based liquid crystalline complexes: synthesis and characterization. Eur Polym J 46(9):1923–1931
19. Qi B, Lu SR, Xiao XE et al (2014) Enhanced thermal and mechanical properties of epoxy composites by mixing thermotropic liquid crystalline epoxy grafted graphene oxide. Express Polym Lett 8(7):467–479
20. Kim JY, Kang SW, Kim SH et al (2005) Deformation behavior and nucleation activity of a thermotropic liquid-crystalline polymer in poly(butylene terephthalate)-based composites. Macromol Res 13(1):19–29
21. Selvarasu C, Kannan P (2015) Synthesis, characterization of azobenzene and cinnamate ester based calamitic liquid crystalline compounds and their photoresponsive properties. J Mol Struct 1092:176–186
22. Lu SR, Li SR, Yu JH et al (2013) Epoxy nanocomposites filled with thermotropic liquid crystalline epoxy grafted graphene oxide. RSC Adv 3(23):8915–8923
23. Li X, Wen R, Zhang Y et al (2009) Photoresponsive side-chain liquid crystalline polymers with an easily cross-linkable azobenzene mesogen. J Mater Chem 19(2):236–245
24. Alici O, Karatas I (2015) Novel liquid crystal aldoximes and aldoxime ethers: synthesis, characterization and liquid crystal behavior. J Mol Liq. doi:10.1016/j.molliq.2015.04.016
25. Liu Q, Wang J, Dong YD et al (2015) Using a selective cadmium-binding peplipid to create responsive liquid crystalline nanomaterials. J Colloid Interface Sci 449:122–129
26. Jaisankar SN, Nelson DJ, Brammer CN (2009) New synthesis and characterization of ionic polyurethane-urea liquid crystals. Polymer 50(20):4775–4780
27. Zeng C, Lu SR, Song LF et al (2015) Enhanced thermal properties in a hybrid graphene-alumina filler for epoxy composites. RSC Adv 5(45):35773–35782
28. Chen SH, Lv SF, Hou GX et al (2015) Mechanical and thermal properties of biphenyldiol formaldehyde resin/gallic acid epoxy composites enhanced by graphene oxide. J Appl Polym Sci 132(41):42637
29. Wu S, Ladani RB, Zhang J et al (2015) Aligning multilayer graphene flakes with an external electric field to improve multifunctional properties of epoxy nanocomposites. Carbon 94:607–618
30. Sahoo SK, Mohanty S, Nayak SK (2015) Study on the effect of woven sisal fiber mat on mechanical and viscoelastic properties of petroleum based epoxy and bioresin modified toughened epoxy network. J Appl Polym Sci 132(43):42699
31. Pan L, Lu S, Xiao X et al (2015) Enhanced mechanical and thermal properties of epoxy with hyperbranched polyester grafted perylene diimide. RSC Adv 5(5):3177–3186
32. Saha M, Tambe P, Pal S et al (2015) Effect of non-ionic surfactant assisted modification of hexagonal boron nitride nanoplatelets on the mechanical and thermal properties of epoxy nanocomposites. Compos Interfaces 22(7):611–627
33. Tong W, Zhang Y, Zhang Q et al (2015) Achieving significantly enhanced dielectric performance of reduced graphene oxide/polymer composite by covalent modification of graphene oxide surface. Carbon 94:590–598
34. Ashori A, Rahmani H, Bahrami R (2015) Preparation and characterization of functionalized graphene oxide/carbon fiber/epoxy nanocomposites. Polym Test 48:82–88
35. Meng F-B, Cui Y, Chen H-B et al (2009) Phase behaviors of comb-like liquid crystalline polysiloxanes containing fluorinated mesogenic units. Polymer 50(5):1187–1196
36. Liu P, Yao Z, Zhou J (2015) Preparation of reduced graphene oxide/Ni0·4Zn0·4Co0·2Fe_2O_4 nanocomposites and their excellent microwave absorption properties. Ceram Int 41(10):13409–13416
37. Zhang J, Sun Y, Wu Q et al (2014) Preparation of graphene oxide-based surface plasmon resonance biosensor with Au bipyramid nanoparticles as sensitivity enhancer. Colloids Surf B 116:211–218
38. Song SH, Park KH, Kim BH et al (2013) Enhanced thermal conductivity of epoxy-graphene composites by using non-oxidized graphene flakes with non-covalent functionalization. Adv Mater 25(5):732–737
39. Meng FB, Du C, Zhou NY et al (2013) Synthesis and characterization of fluorinated liquid-crystalline elastomers containing chiral liquid-crystalline crosslinking units. Eur Polym J 49(10):3392–3401
40. Godzwon J, Sienkowska MJ, Galewski Z (2012) Liquid-crystalline polymorphism of 4-heptyloxybenzylidene-4′-alkyloxyanilinesand their phase equilibrium with 4-octyloxyphenyl 4-nitrobenzoate. Thermochim Acta 531:75–82

41. Lagerwall JPF, Scalia G (2012) A new era for liquid crystal research: applications of liquid crystals in soft matter nano-, bio- and microtechnology. Curr Appl Phys 12(6):1387–1412
42. Wang F, Cao H, Li K et al (2012) Control homogeneous alignment of chiral nematic liquid crystal with smectic-like short-range order by thermal treatment. Colloids Surf A 410:31–37
43. Coleman JN, Khan U, Blau WJ et al (2006) Small but strong: a review of the mechanical properties of carbon nanotube–polymer composites. Carbon 44(9):1624–1652
44. van Rooyen LJ, Karger-Kocsis J, Kock LD (2015) Improving the helium gas barrier properties of epoxy coatings through the incorporation of graphene nanoplatelets and the influence of preparation techniques. J Appl Polym Sci 132(39):42584
45. Zhang QX, Yu ZZ, Xie XL et al (2004) Crystallization and impact energy of polypropylene/CaCO3 nanocomposites with nonionic modifier. Polymer 45(17):5985–5994
46. Braun U, Balabanovich AI, Schartel B et al (2006) Influence of the oxidation state of phosphorus on the decomposition and fire behaviour of flame-retarded epoxy resin composites. Polymer 47(26):8495–8508
47. Yuan ZK, Yu JH, Rao BL et al (2014) Enhanced thermal properties of epoxy composites by using hyperbranched aromatic polyamide grafted silicon carbide whiskers. Macromol Res 22(4):405–411
48. Yasmin A, Daniel IM (2004) Mechanical and thermal properties of graphite platelet/epoxy composites. Polymer 45(24):8211–8219
49. Gojny FH, Wichmann MHG, Fiedler B et al (2006) Evaluation and identification of electrical and thermal conduction mechanisms in carbon nanotube/epoxy composites. Polymer 47(6):2036–2045
50. Naebe M, Wang J, Amini A et al (2014) Mechanical property and structure of covalent functionalised graphene/epoxy nanocomposites. Sci Rep 4:4375
51. Biswas S, Shahinur S, Hasan M et al (2015) Physical, mechanical and thermal properties of jute and bamboo fiber reinforced unidirectional epoxy composites. Procedia Eng 105:933–939
52. Li Y, Zhu H, Zhu S et al (2015) Hybridizing wood cellulose and graphene oxide toward high-performance fibers. NPG Asia Mater 7(1):150